International Journal of Computing and Digital Systems
ISSN (2210-142X)
Int. J. Com. Dig. Sys. 15, No.1 (Mar-2024)

http://dx.doi.org/10.12785/ijcds/150176

PrinciResNet Brain Tumor Classification Technique for Multimodal Input-level Fusion Network

Padma Usha. M[1], Kannan. G[1], Sai Akshay. S[1], Giri. S[1] and Shaik Mohammed Huzaifa[1]

[1]*Department of Electronics and Communication Engineering, B S Abdur Rahman Crescent Institute of Science and Technology, Chennai, India*

Received 4 May 2023, Revised 14 Feb. 2024, Accepted 24 Feb. 2024, Published 1 Mar. 2024

Abstract: Brain tumors are a leading cause of mortality in India, with over 28,000 cases reported annually, resulting in more than 24,000 deaths per year as per the International Association of Cancer Registries. Early detection, segmentation, and accurate classification are crucial in effective tumor analysis, and various algorithms have been developed to achieve this. This study proposes a new approach for the detection and classification of Meningioma and Sarcoma brain tumors using both single slices of MRI and CT, as well as input-level fused images of MRI & CT. Our approach involves the implementation of the PrinciResNet16 model for classification of brain tumors. This model is based on Principal Component Analysis (PCA) and ResNet techniques. We report that our approach significantly improves the accuracy, sensitivity, and specificity parameters to 99%, 95%, and 95%, respectively, based on a dataset of 600 fused slices and 1000 single slices obtained from reputable sources. Our findings hold promise for better brain tumour detection and therapy, which are a significant cause of mortality globally.

Keywords: PCA, ResNet, Skip connection, Brain tumor, CT, MRI

I. INTRODUCTION

Brain tumors are a relatively rare occurrence, with approximately seven diagnoses per 100,000 individuals globally each year, constituting 2 % of all tumor cases. Notably, the mortality rate is most elevated among children below the age of 12 and ranks as the tenth highest among adults. Consequently, a prominent focus of ongoing medical research related to brain tumors is the precise localization, segmentation, and classification of these tumors [1]. One of the primary challenges in the classification and segmentation of brain tumors lies in the uncertainty associated with their shapes and sizes. Various types of tumors are commonly found within the brain, including Meningioma, Glioma, and Pituitary tumors [2]. Additionally, metastatic tumors like sarcoma and Gliosarcoma can also be located in different regions of the brain. To address this, Artificial intelligence-based classification techniques for brain tumor images are appropriate and can be categorized into two main approaches namely, machine learning and deep learning [3]. Machine learning can be further divided into unsupervised and supervised learning. Machine learning has the potential to improve the accuracy of medical picture classification, which could have important consequences for cancer detection and therapy. Deep learning techniques, on the other hand, can be broadly grouped into three categories such as fully connected networks, Convolutional Neural Networks (CNNs), and Recurrent Neural Networks (RNNs). Among these, CNNs are the most effective technique for tasks such as object recognition and classification [4]. Currently, deep learning methods hold greater prominence in achieving accurate classifications, as they possess self-learning capabilities, which are particularly advantageous when there is a large dataset [1]. ResNet, one of CNN architectures employs skip convolution to overcome the gradient vanishing problem and is well utilized for Unet architecture to increase its efficiency. A hybrid model is preferred in which two deep-learning models are combined to improve the classification accuracy [5]. Existing techniques use more layers to achieve high accuracy which in turn increases the complexity of the model. Hence, achieving high accuracy in the classification of tumors with a minimum number of layers is a challenging task. Also, high accuracy leads to early detection of tumors [6]. It is vital to provide the diagnostic system with every information that is present in the lesion to develop a powerful diagnostic system that will appropriately classify brain tumors [7]. The promise of artificial intelligence approaches is to improve medical

E-mail address: padmausha@crescent.education, kannan@crescent.education, saiakshayns@gmail.com, girisalapathi@gmail.com, huzaifashaik615@gmail.com

image analysis for disease diagnosis and detection[8].Our proposed model addresses this by improving the accuracy of classification by using a minimum number of layers whereas other techniques discussed use more number of layers to achieve high classification accuracy.

Apart from accurate localization, segmentation, and brain tumor classification, the reduction of redundant pixels of input image is considered an important part of image processing which in turn improves the efficiency of the process. The impact of decorrelation is the energy compaction of images after which processing is made easier. Various techniques exist for obtaining decorrelated images. One of the best methods which is a statistical method in image processing to make the image more energy compacted and decorrelated is Principal component analysis (PCA). This method is based on obtaining Eigen values and Eigen vectors of an image. PCA algorithm on MRI images was combined with the application of the clustering algorithm [9]. There are various methods of PCA have been implemented. The hybrid attention block improves the characteristics that each encoder individually obtains from the respective imaging modality's low-level features. The decoder restores the results of the pixel-level segmentation after combining with the decoder path's high-level semantics through skip convolution [10]. PCA and Superpixels are used to extract key features that enable the precise detection of brain malignancies. It increases data interpretability with minimal data loss [11]. Accuracy rates rise when feature vectors are restricted to the PCA's preferred component [12]. PCANet extracts features from images using a two-phase convolutional neural network (CNN). The authors show how PCANet works on different benchmark datasets and highlight its potential for practical applications in computer vision and image analysis [13]. PCA's efficiency in decreasing the computational complexity of image processing while keeping the image's significant visual qualities. This can significantly increase the efficiency of image analysis and related applications [14]. PCA has been used in medical image processing for dimensionality reduction, noise reduction, and image segmentation. According to the findings, PCA could be a beneficial method for increasing the accuracy and efficiency of medical image analysis and associated applications [15]. The proposed method employs the implementation of PCA technique for redundancy removal from the input image in a preprocessing stage for multimodal as well as single modal images whereas other methods implement feature extraction and prevent information loss only for single modal images. The findings show that the suggested method could have important implications for efficient and accurate brain tumor diagnosis utilizing medical imaging. Our proposed model mainly implements the brain tumor classification of Meningioma and Sarcoma, CT, MRI and, its fused images using PrinciResNet16 architecture. This model addresses

1) PCA-based preprocessing of an input image is carried out for redundancy removal.

2) Modeled PrinciResNet architecture with 16 layers and 5 skip convolutions with a reduction in computation time with high accuracy.

3) Effective classification is performed for single slices as well as fused slices of MRI/CT for Meningioma and Sarcoma brain tumor types.

This paper is structured as follows: Initially, the introduction segment provides the current scenario of the proposed problem and research gap. Also, this section discusses existing methods and conveys the proposed method to fill the research gap. The next section is materials and methods which describes the detailed explanation of the data implemented for this research and the detailed explanation of the proposed method. Results and discussions are in the next section.

II. METHODOLOGY

A *Data Collection and Preprocessing*

a) *Dataset*

The PrinciResNet16 method consists of the following sequences: Pre-processing involving resizing and filtering, redundancy removal using PCA, and classification using the ResNet technique. This method was implemented in MATLAB 2019a version with system specifications as Core i9 Processor 3.7 GHz, Asus ROG Strix Z490 Motherboard 64 GB RAM, Nvidia Quadro P4000 8GB GPU. Our proposed approach involves the utilization of two distinct imaging modalities, specifically MRI and CT scans, and the fused images of MRI-CT focusing on both identical and differing brain tumor types, namely Meningioma and Sarcoma. MRI-CT images are fused using a pixel-level maximum method of fusion. [15]. Meningioma is an example of a primary brain tumor and Sarcoma is an example of a metastatic brain tumor. Datasets are used to validate the proposed methodology and were obtained from two separate databases www.med.harvard.edu/AANLIB/home.html [16] and www.kaggle.com [17]. The details of the downloaded images are outlined in Table I. From the Medharvard database, MRI images in various sequences, including T1, T2, Gadolinium, and proton density slices, and the Kaggle database with MRI T1 and T2 images are obtained. Meningioma and Sarcoma images are acquired from two different patients on Medharvard website. Both image databases contain axial slices of brain tumor images. Before using

these images for analysis, preprocessing has been performed to enhance the suitability of images for further processing in the next stage.

b) *Preprocessing*
The initial preprocessing step involved resizing the images. The Medharvard images originally had a resolution of 256x256 and were in Graphics Interchange Format (GIF). We resized them to a spatial resolution of 224x224 and converted their file format to Joint Photographic Experts Group (JPEG). Similarly, the Kaggle images were also resized to 224x224.
Following that, a filtering process is employed to eliminate noise from the images. In this regard, a 3x3 median filter is utilized, a widely accepted technique in biomedical images for effectively eliminating salt and pepper noise [18]. This method is highly applicable to images obtained from databases as well as real-time datasets acquired from hospitals and research centers. Furthermore, the median filter is characterized as a non-linear filter, meaning that its output is not directly dependent on the input in a linear fashion. This characteristic makes it particularly well-suited for biomedical images, where the presence of lesions is often uncertain.
The PrinciResNet16 approach integrates Principal Component Analysis (PCA) to reduce redundant information within image data, and it employs a ResNet16 model for the task of tumor classification. Fig. 1 illustrates the flow diagram of the PrinciResNet16 model.

B *Principal Component Analysis (PCA)*
Principal Component Analysis (PCA) is a commonly used method for reducing dimensionality, and it is particularly effective for reducing the dimensionality of the data [19]. It converts correlated images into uncorrelated images thus in turn decreasing the redundancy of the input images. Eigenvectors are found in PCA of input images which gives the direction of pixels having a higher variance. An image is decomposed into various components in which the principal component has energy compact and decorrelated features with a high reduction in its dimensions [14]. In the PrinciResNet16 method, the first principal component is considered a training image for the ResNet16 model. Mathematically, modes of PCA can be derived as follows,

- Consider an original image P which consists of n contours and Covariance matrix C of the original image P is given by,

$$C = \frac{1}{n}\sum_{a=1}^{n}(P_a - \overline{P})(P_a - \overline{P})^T \tag{1}$$

$$\bar{P} = \frac{1}{m}\sum_{i=1}^{m} P_i \tag{2}$$

$\bar{P}$ $\rightarrow$ Mean value of the original image

$(P_(a) - \bar{P}) \rightarrow$ Shape distortion
Covariance matrix from (1) is represented as,

$$C = \begin{bmatrix} \text{cov}(x,x) & \text{cov}(x,y) & \text{cov}(x,z) \\ \text{cov}(y,x) & \text{cov}(y,y) & \text{cov}(y,z) \\ \text{cov}(z,x) & \text{cov}(z,y) & \text{cov}(z,z) \end{bmatrix} \tag{3}$$

Cov(x,x) , Cov(y,y) & Cov(z,z) $\rightarrow$ Diagonal elements showing variance between the same variables.

Cov(x,y),Cov(x,z)...Cov(z,y) $\rightarrow$ Off-diagonal elements showing variance between one variable with another variable.

This covariance matrix element gives the type of correlation such as positive correlation, negative correlation, and uncorrelation between the variables. Along the diagonal correlation is almost 1 and other elements provide various values that indicate the type of correlation between the variables. Positive values between variables indicate a positive correlation and negative values signify an inverse correlation.

PCA makes the correlated matrix into an uncorrelated matrix by finding eigenvectors $[S_1, S_2 - - - - - S_k]$ of eigenvalues as $, - - - - - -, \lambda_k$ where $\lambda_1 \geq \lambda_2 \geq \lambda_3 \geq - - - - \geq \lambda_k$ of Covariance matric C and k is the number of dimensions or features of an input image.

The new axes S_k in feature space leads to various directions of variation that are mutually not correlated and its variability is defined by the principal mode of variation. Hence, due to this number of degrees of freedom has consistently decreased [20].

An image model can then be represented in terms of principal component axes as,

$$P^* = P * S_k \tag{4}$$

is an uncorrelated version of the original image P plotted in a new uncorrelated space.

Considering only the foremost modes of variation, dimensionality is reduced which in turn reduces redundancy in the original image. The proposed PrinciResNet16 method involves working with images to construct a 3x3 covariance matrix. This matrix is created by arranging three eigenvectors, denoted as S_1, S_2

TABLE I. TUMOR CLASSIFICATION LABEL AND ITS COUNT

Database	Classification Label	Count
Kaggle	CT Tumor Meningioma	200
Kaggle	CT Tumor Sarcoma	198
Kaggle	MRI Tumor Meningioma	176
Kaggle	MRI Tumor Sarcoma	276
Medharvard	MRI CT Fused	600
Kaggle	No Tumor	150
	Total image slices	1600

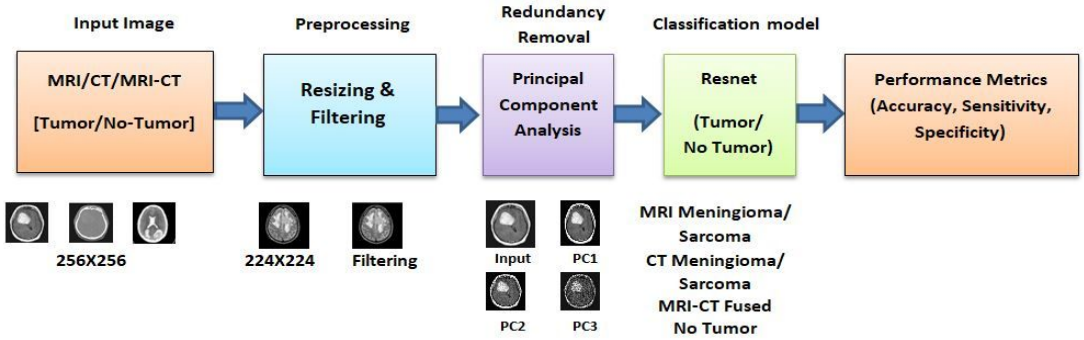

Figure 1. Flow diagram of the PrinciResnet16 technique

, and S_3 corresponding to eigenvalues λ_1, λ_2 , and λ_3 in descending order. Using these eigenvectors, we obtain the first, second, and third Principal Components, denoted as IPC1, IPC2, and IPC3, respectively. In the process of Principal Component Analysis (PCA), IPC1 is generated first, and IPC2 is positioned orthogonal to IPC1.

C *Deep learning Model- PrinciResNet16*

The process flow shown in Fig. 2 illustrates the successive stages of the proposed PrinciResNet16 algorithm. It commences with image resizing and filtering to prepare the data. PCA is applied to significantly reduce redundancy in the data [20]. CNN ResNet architecture with skip connections comprises the convolutional layer, ReLU layer, and pooling layer. Notably, skip connections, introduced in Fig. 3, play a vital role. After convolutional operations, the output is flattened into a suitable format for further processing. The flattened data is transferred to a fully connected layer, where it interacts with neuron cells for tumor classification. The neural network uses the resulting column vector as input to classify the data into six different categories: MRI Meningioma, MRI Sarcoma, CT Meningioma, CT Sarcoma, MRI-CT fused image, and no tumor.

In the second flow diagram in Fig. 2, the process commences with the input of the principal component, IPC1, with dimensions 224X224. This input is given to the PrinciResNet16 model which consists of fifteen convolution layers, five skip connections, and thus five residual blocks. To mitigate issues like vanishing gradients and exploding gradients, skip connections are introduced [21]. These connections allow input from specific layers to bypass intermediate layers and pass directly to layers located two steps ahead. This architectural design helps to address gradient-related challenges in deep neural networks. Each residual block consists of 11 internal layers [22].

The first residual block consists of convolution layer (conv1), batch normalization layer(bn1),relu layer(rel1) and maximum pooling layer(mp1) followed by second convolution layer(conv2), batch normalization(bn2), relu layer(rel2) subsequently followed by third convolution layer(conv3), batch normalization layer(bn3), relu layer(rel3) and here comes the role of skip connection which is generated by adding the output from rel1 with output from rel3 output such that the activation size of rel1 should be equal to activation size of output from rel3. Table II represents the layer description of each layer i.e., it conveys the size of the kernel used in that particular layer followed by several filters used in that layer. These filters are responsible for learning features like line detection,

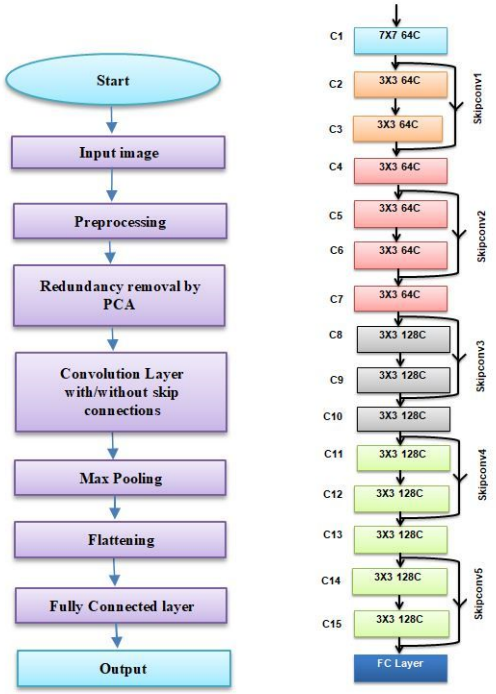

Figure 2. Process flow of PrinciResnet16 model and its layers flow diagram

edge detection, point detection, and so on. The more the number of filters, the more the learning of features by the model.

Let us consider from Fig. 3, input as Y and the expected output as H(Y), and mapping learned by the network as F(Y). Then the mapping learned with residual block is given by

$$F(Y) = H(Y) - Y \tag{5}$$

Table II offers comprehensive components of the architecture for a single residual block in the context of a neural network designed for image classification. This block consists of a total of 16 layers. The table provides essential details, including the layer name, a brief description of its function, the input image size it operates on, and the size of the filter kernel employed. These ResNet block layers are repeated up to the fifth residual block. Notably, each convolution operation within this block serves as a residual function, where the input is element-wise added to the output feature maps produced by the convolutional operation. This strategic addition of skip connections accelerates the convergence of the network. Moreover, these skip connections effectively decrease the problem of degradation that commonly arises in deep networks. This ensures that the network can effectively train and learn complex features and addresses the degradation issue that arises with such deep networks [23].

III. RESULTS AND DISCUSSION

Initially, the PCA method is implemented to input images to reduce the redundancy of the same. In Fig. 4, the three components of six classifications of input images were shown after median filtering. The principal component IPC1 is given as input to the deep learning algorithm which is ResNet16 architecture. By implementing PCA in the input image the significant amount of redundancy has been reduced [14]. Pairplots were plotted in Fig. 6 to compare the pairwise correlations in the original data with those in the main components to judge how well the PCA reduced redundancy and achieved data reduction [24]. We saw that the main components completely removed the connection between the variables contained in the original data, showing a considerable decrease in correlation. Furthermore, the diagonal distribution plots showed that the PCA successfully transferred compressibility-related variance. Our research suggests that the PCA was successful in data compression and redundancy reduction overall.

We can make decisions about which Principal Components to retain and which to discard based on a variance plot, as depicted in Fig. 5. This plot allows us to determine the

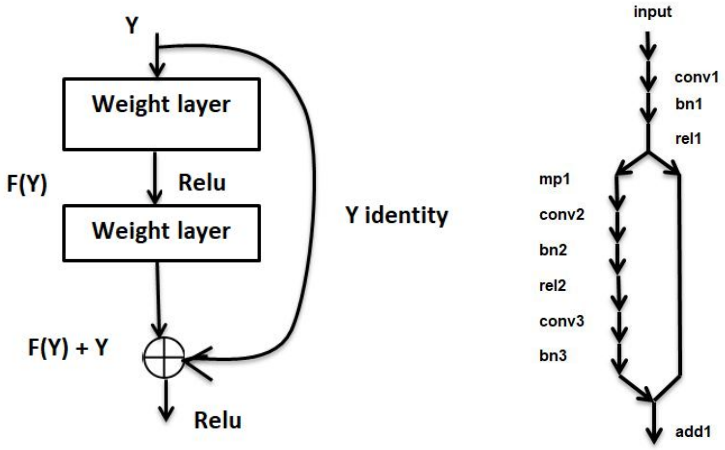

Figure 3. Single Skip connection of ResNet16 architecture

TABLE II. LAYER DESCRIPTIONS

Layer number	Layer name	Layer expansion	Layer Description
1	'input'	Input Image	224x224x1 images with 'zero centers' normalization
2	'conv1'	Convolution	64 7x7x1 convolutions with stride [1 1] and padding option as 'same'
3	'bn1'	Batch Normalization	Normalization in batches of 64 channels
4	'rel1'	ReLU	Rectified Unit
5	'max pool1'	Max Pooling	Pooling 2x2 with padding [0 0 0 0] and stride [2 2]
6	'conv2'	Convolution	64 3x3x64 convolutions with stride [1 1] and 'same' padding
7	'bn2'	Batch Normalization	Normalization in batches of 64 channels
8	'rel2'	ReLU	ReLU
9	'conv3'	Convolution	64 3x3x64 convolutions with padding 'same' and stride [1 1]
10	'bn3'	Batch Normalization	Batch Normalization
11	'add'	Addition	Element-wise addition of 2 inputs
12	'rel3'	ReLU	ReLU
13	'FC'	Fully Connected	6 inter-connected layers
14	'soft max'	Softmax	Softmax function
15	'class output'	Classification Output	Crossentropy with 'CT-NO_TUMOR' and 5 other classes
16	'skip Conv'	Convolution	64 1x1x64 convolutions with padding [0 0 0 0] and stride [2 2]

IPCs that preserve the most information from the original image. In this specific analysis, IPC1 is selected because it retains the maximum amount of information, while IPC2 and IPC3 are disregarded as they contain only a minimal amount of information. To evaluate the redundancy between the original input image and its Principal Component Analysis (PCA) representation, separate pair plots were generated for each. Simultaneously, a pair plot was created for the principal components (PC) of the PCA. This pair plot featured histograms along the diagonal corresponding to IPC1, IPC2, and IPC3 and scatterplots for other rows to visually convey the relationships between variables of the PCs. Upon comparing the pair plot of the input image with that of the PCA's first component, a clear distinction emerged. Variables of input images exhibit a positive correlation, as they tend to increase together. The PCA components displayed minimal correlation among variables, indicating the successful removal of redundancy from the original input data. In contrast, the input column vector exhibited a noticeable correlation among its variables, underscoring the PCA's effectiveness in eliminating redundancy from the input layer data. If we observe Fig. 6, for the reshaped input image matrix in which pixels are kept column-wise with three columns indicating three dimensions, a pair plot of all the columns, and one column versus another column is plotted. Histograms were placed along the diagonal of the pair plot, depicting the distribution of intensity values of each column of the image matrix. The x-axis represented possible intensity values, while the y-axis displayed the frequency of occurrence of these values. The subplot in the ith row, a jth column is the scatterplot of the ith column against the jth column of the reshaped input image matrix. Input image histogram plots for the redundant image whereas the first principal component histogram plots the highly uncorrelated image.

It is evident from Table III, which provides a comparative analysis of the statistical characteristics of PCA components to understand their behavior. Upon analyzing IPC1, IPC2, and IPC3, it becomes apparent that certain parameters, including mean intensity, standard deviation, entropy, and peak signal-to-noise ratio (PSNR), exhibit more favorable values for IPC1. Conversely, IPC2 and IPC3 deviate further from the desired or ideal values [10]. Consequently, IPC1 is chosen for the subsequent training of images in the ResNet16 model. The high value of standard deviation observed in IPC1 across all tumor classifications signifies a considerable level of variance. Examining the table, it is apparent that IPC1 attains the optimal entropy value within the range of 0 to 1. Furthermore, in terms of PSNR, considering the peak value as 65535 the ideal range varies from 20 dB to 50 dB for which IPC1 falls in this ideal range, whereas the other components exhibit substantial deviations from the preferred statistical parameter values. Additionally, for the input image, I also, mean intensity, standard deviation, and entropy are observed.

A *Training Phase of the PrinciResnet16 model*

The PrinciResNet16 model was trained using a dataset consisting of 1600 images, and its training involved various parameters such as the number of epochs, which ranged from 5 to 50, and a learning rate set at 0.01. Performance evaluation was conducted using metrics like Accuracy, Sensitivity, and Specificity. Additionally, the model's efficiency was compared to that of the ResNet model, with computation time also being recorded.

In the following section, we discuss training progress and the learning stages of activation layers specifically for Meningioma and Sarcoma [23]. The training progress encompasses the model's performance at each epoch, including training accuracy, training loss, validation accuracy, and validation loss. The goal during the training phase is to iteratively adjust these parameters to achieve the highest accuracy while minimizing loss within the predefined number of epochs. It's worth noting that 30% of the dataset was allocated for validation data, while the remaining 70% was designated for the training dataset. The training phase involves the model's gradual learning process as it adapts to the various filters specified in the model architecture. This learning progression is illustrated in Fig. 8 for Meningioma and Sarcoma tumor types [28].

This describes the activation images at different stages of a convolutional neural network, specifically highlighting Convolution Layer 1, ReLU Layer 1, Pooling Layer 1, Convolution Layer 2, and ReLU Layer 2. In Convolution Layer 1, features like lines, edges, and points are extracted. ReLU Layer 1 then transforms all negative values to zero, enhancing the activation map. Pooling Layer 1 reduces the pixel count by a factor of 4:1, serving as a dimensionality reduction technique, while using various filters to capture brain tumor features. Moving to Convolution Layer 2, its activation image extracts even more intricate features compared to Convolution Layer 1 [3]. The ReLU Layer 2 delves deeper into feature extraction, as evidenced by the feature maps in ReLU Layer 1. Pooling Layer 1, on the other hand, provides a clearer outline of the tumor compared to ReLU Layer 1.

Among the various feature maps produced in Convolution Layer 1, the most prominent channel of Convolution Layer 1 highlights the map where the most features are extracted from its own set of filters. As we examine deeper into the network's layers (e.g., 1, 2, 3,

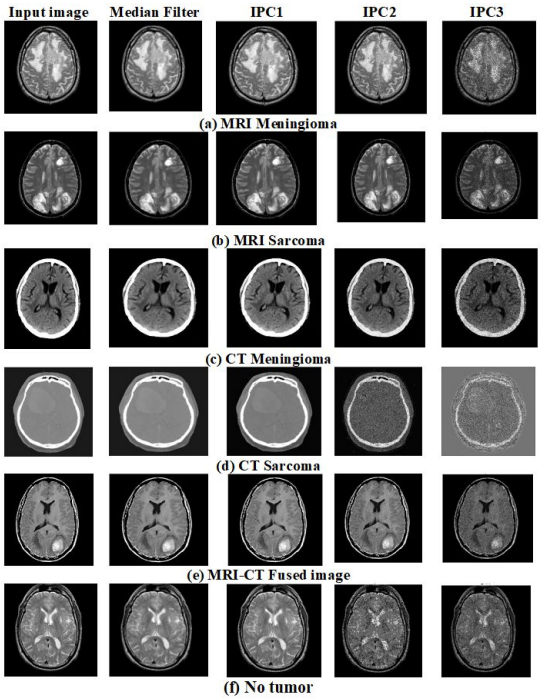

Figure 4. Input images and its principal components of classes of brain tumor

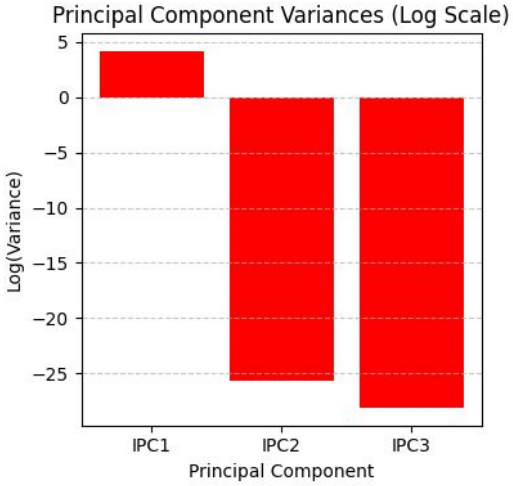

Figure 5. Comparison of information content for the first three principal components

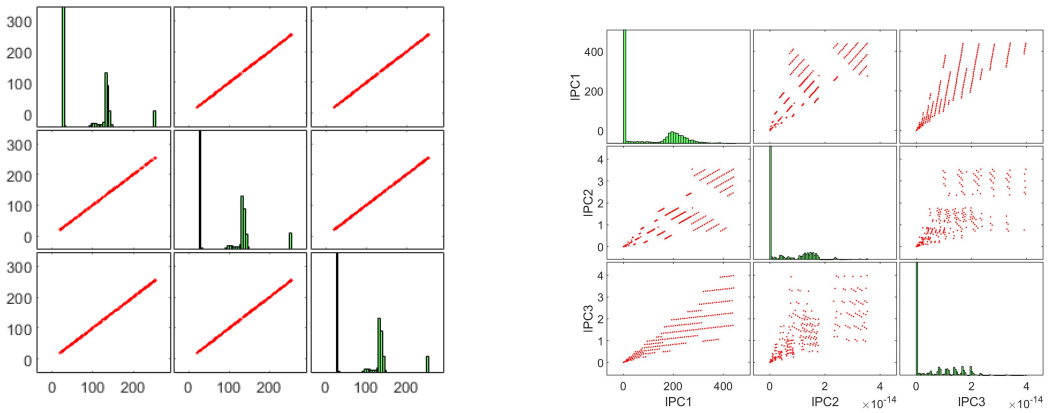

Figure 6. Histogram and correlation of input image and its Principal components IPC1, IPC2 & IPC3

TABLE III. STATISTICAL PARAMETERS OF PCA FOR DIFFERENT CLASSES OF BRAIN TUMOR

Statistical Parameters	**Mean Intensity**				**Standard Deviation**			
Tumor class	***I***	***IPC1***	***IPC2***	***IPC3***	***I***	***IPC1***	***IPC2***	***IPC3***
Meningioma CT	65.8652	114.082	7.68E-15	7.72E-15	80.9755	140.2544	1.02E-14	1.05E-14
Meningioma MRI	57.4101	99.4372	3.19E-14	6.38E-15	73.089	126.5945	4.09E-14	8.73E-15
Sarcoma CT	66.2815	114.8029	2.24E-14	7.79E-15	84.8282	146.9275	2.91E-14	1.08E-14
Sarcoma MRI	41.7116	72.2466	2.78E-14	4.63E-15	57.8104	100.131	3.87E-14	6.87E-15
Fused image	60.7932	105.2969	2.03E-14	6.78E-15	70.1329	78.5588	2.37E-14	8.40E-15
No tumor	62.1358	107.6224	6.87E-15	6.93E-15	66.4101	115.0262	8.22E-15	8.00E-15

Statistical Parameters	**Entropy**				**Peak SNR (dB)**		
Tumor class	***I***	***IPC1***	***IPC2***	***IPC3***	***IPC1***	***IPC2***	***IPC3***
Meningioma CT	0.752	0.993	0	0	32	2.6027	2.6027
Meningioma MRI	0.62	0.9896	0	0	33.5	3.215	3.215
Sarcoma CT	0.702	0.9973	0	0	35	3.2838	3.2838
Sarcoma MRI	0.821	0.9946	0	0	31.4	3.4014	3.4014
Fused image	0.658	0.9847	0	0	32.6	2.5447	2.5447
No tumor	0.712	0.9849	0	0	37	2.4239	2.4239

TABLE IV. COMPUTATION TIME OF PRINCIRESNET16 MODEL WITH RESNET MODEL

	Training with ResNet	**Training With PrinciResNet16**
Epoch	**Computation time (sec)**	
5	40	33
10	47	40
15	63	59
20	102	95
25	130	122
30	154	153
35	186	186
40	215	207
45	253	248
50	336	320

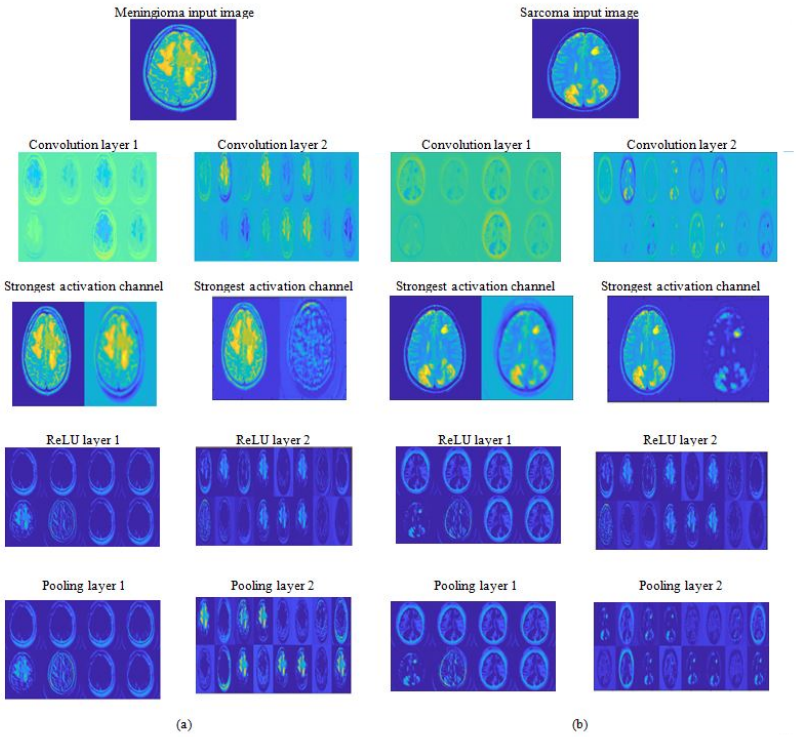

Figure 7. Visualization of activation feature maps of Meningioma and Sarcoma for layer 1 and layer 2

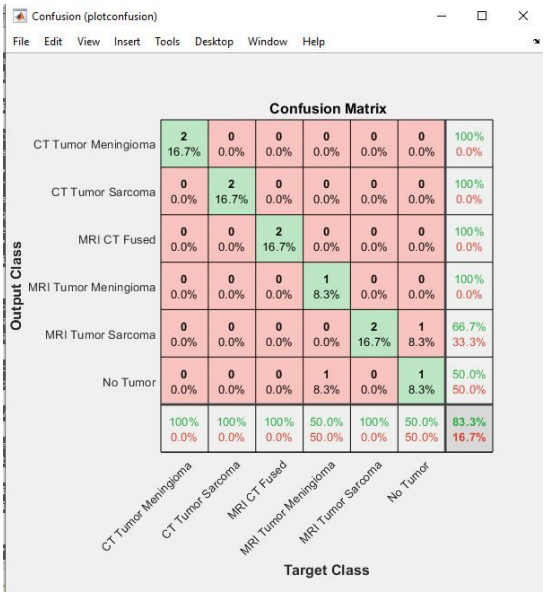

Figure 8. Confusion matrix for brain tumor classification

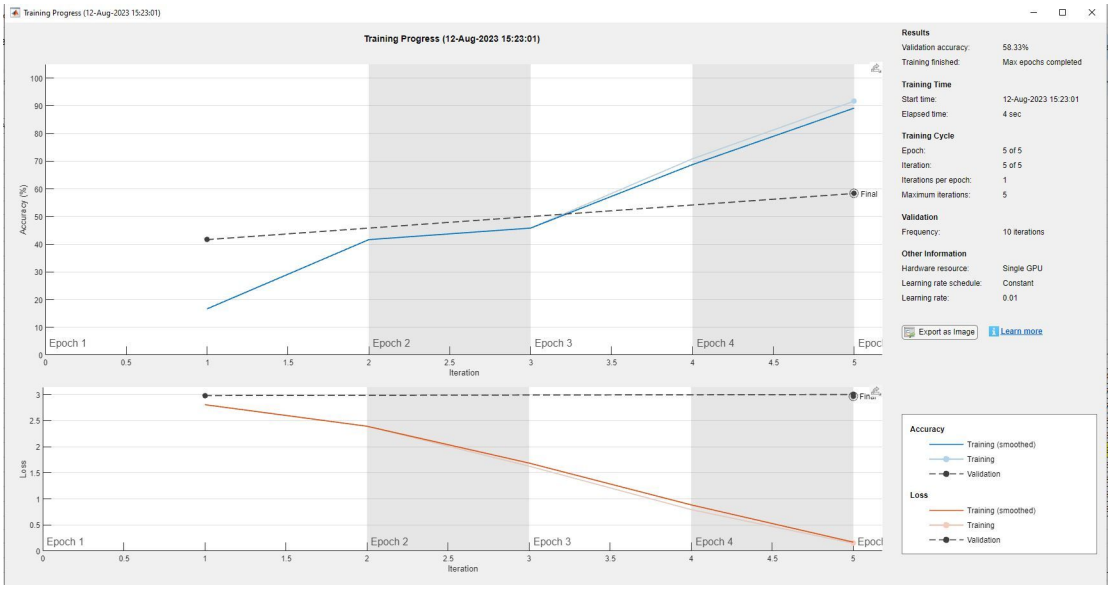

Figure 9. Training and Validation Accuracy and Loss for the Epoch 5

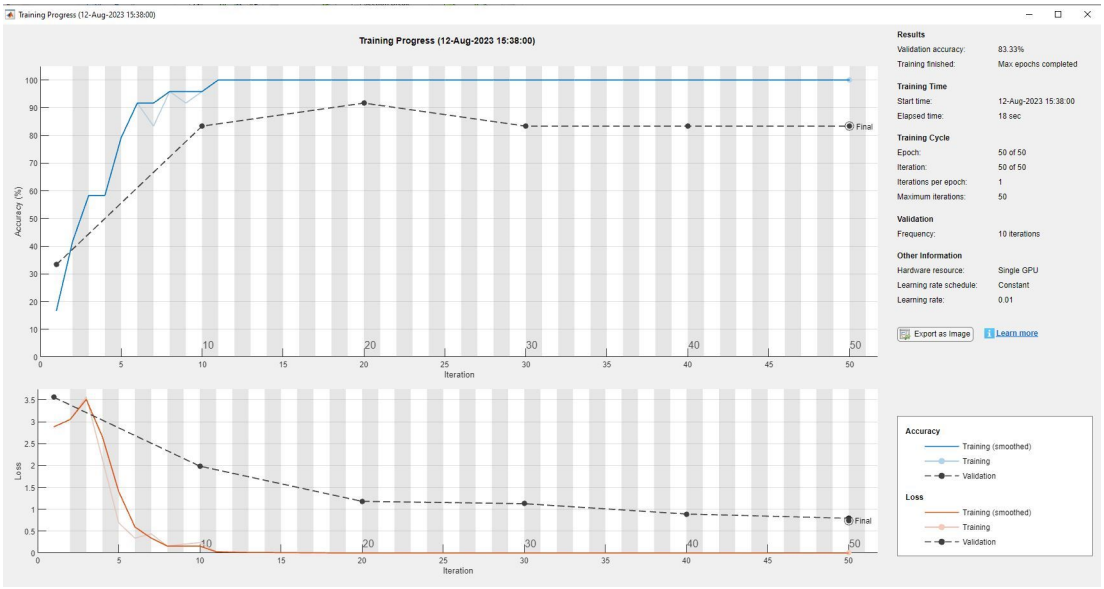

Figure 10. Training and Validation Accuracy and Loss for the Epoch 50

TABLE V. METHODS IMPLEMENTED FOR BRAIN TUMOR CLASSIFICATION AND PERFORMANCE METRICS

Reference	**Method Implemented**	**Performance Metrics**
Proposed	PrinciResNet16	Accuracy - 99%Sensitivity - 95%Specificity - 95%
[25]	DWT + PCA + ANN	Accuracy - 97%Sensitivity - 95%Specificity - 94%
[26]	LeaSE-DARTS	Accuracy - 91%Specificity - 98%
[27]	Data Augmentation Method	Sensitivity - 91%
[22]	EADL-BTMIC Model	Accuracy - 98%Specificity - 99%
[5]	Hybrid GoogLeNet	Accuracy - 99%

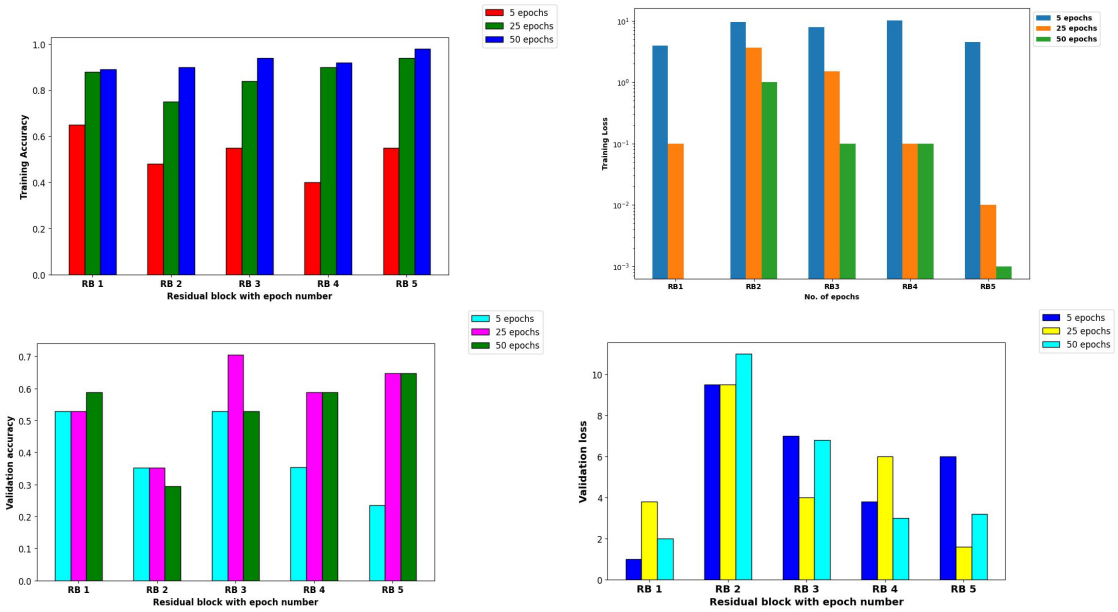

Figure 11. Training accuracy and loss, Validation accuracy and loss from 1st residual block to 5th residual blocks for 5, 25, and 50 epochs respectively.

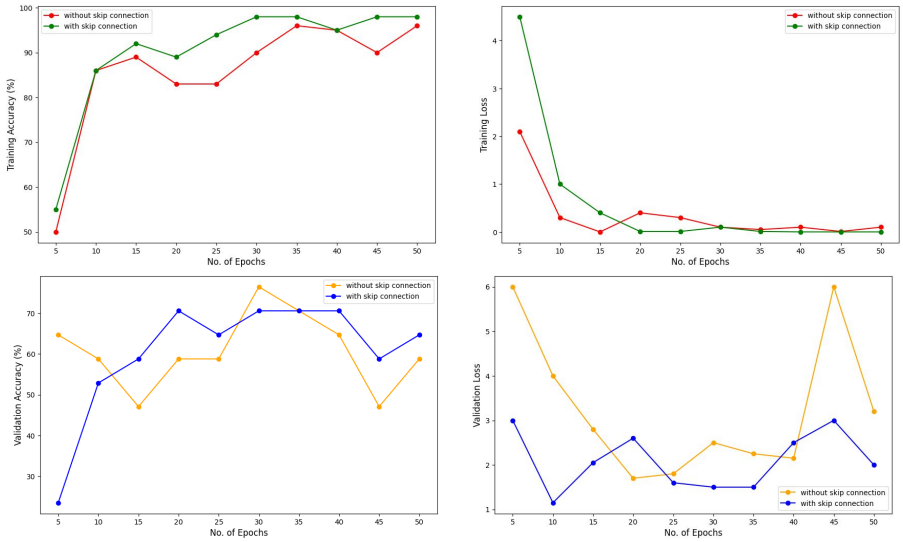

Figure 12. Comparison of training accuracy, training loss, validation accuracy, and validation loss for without and with skip connection from 5th epoch to 50th epoch.

etc.), the depth of feature extraction increases. Before incorporating skip connections, each batch of layers consists of a sequence involving a convolution layer, ReLU layer, pooling layer, and batch normalization. Skip connections significantly enhance the potential for convergence compared to handling a single batch of layers without them. The learning patterns were observed for both Meningioma and Sarcoma cases [23].

The training progress for a single residual block is illustrated in Fig. 9 and Fig. 10, representing the cases where the maximum number of epochs is set to 5 and 50, respectively. In the scenario with a minimal number of epochs (5), the training accuracy remains below 50%. However, as the number of epochs increases, the accuracy steadily improves, eventually reaching a maximum of 99%. This observation demonstrates that higher epoch counts correlate with increased accuracy. Focusing on the loss parameter, when the number of

epochs is limited to 5, this parameter reaches its peak value at 80%. However, with an increase in the number of epochs, the loss parameter gradually diminishes, approaching nearly zero.

In Fig. 8, a confusion matrix has been generated for the single residual block model, classifying data into six distinct categories in brain tumor classification. The diagonal elements within this matrix correspond to the true positives for all six classification categories.

a) *Performance Metrics for validating the proposed algorithm*
An algorithm's efficiency is estimated by finding out various performance metrics. For the proposed algorithm, performance metrics such as accuracy followed by sensitivity, specificity, and computation time were calculated. The definitions of the calculated metrics are given below,

- Accuracy (A)
  It is given by the number of accurate valuations to the number of all valuations. Here, the number of tumor cases detected correctly to the total number of detection cases.
$$A = \frac{No.\,of\,accurate\,valuation}{No.\,of\,all\,valuation} \tag{6}$$

- Sensitivity (S_n)
  It is given by the true positive count to the count of all positive valuations. It is a sub-classification of accuracy such that it is the number of actual positive cases of tumor to the number of positive cases of tumor.
$$S_n = \frac{No.\ of\ true\ positive\ valuations}{No.\ of\ all\ positive\ valuations} \tag{7}$$

- Specificity (S_p)
  It is given by the number of true negative valuations to the number of all negative valuations. It is the number of actual non-tumor cases to the total number of non-tumor cases.
$$S_p = \frac{No.\ of\ true\ negative\ valuations}{No.\ of\ all\ negative\ valuations} \tag{8}$$

The study examined the performance of the network model from single epoch to multiple epochs such as 5, 25, and 50, it is clear from Fig. 11 represents training accuracy touches the peak point at the 50th epoch for ResNet blocks from one to five whereas validation accuracy has its peak point for single residual block. Additionally, training loss is almost zero for the 50th epoch for the fifth residual block, and validation loss is minimal at the 25th epoch of the fifth residual block. From this analysis, it is inferred that as residual block and epoch number increase desirable performance is achieved for the model. The analysis can be further extended to a comparison of the same performance metrics as indicated above with epoch numbers varying from 5 to 50 epochs whereas earlier analysis has been chosen only for selective epochs such as 5, 25, and 50 which indicates the lowest, moderate, and highest epoch. Fig. 12 represents the line plots for comparison of performance metrics. As understood from the previous analysis, in this also residual block 5 at the 50th epoch outperforms other ResNet blocks and epochs. Overall, this analysis demonstrates the effectiveness of the ResNet architecture in improving the accuracy and reducing the loss in deep learning models. It also highlights the importance of choosing the appropriate number of residual blocks to achieve the best performance.

Training Accuracy gradually increases from the first to the fifth residual block. When simulated from 5 to 50 epochs, these five residual blocks exhibit higher training accuracy than validation accuracy. Training loss appears to be less than validation loss and, in some cases, zero. Regardless of residual blocks, the parameters appear to be unpromising from 5 to 25 epochs, but promising from 30 to 50 epochs. We acquire the lowest validation loss and highest validation accuracy in the 5th Residual Block.

Table IV presents a comparison between the computation times of the PrinciResNet16 and ResNet models, offering insights into the relative speed of these algorithms within specified configurations. It is a metric employed to measure the duration required for an algorithm to finish its computational tasks. As the number of epochs increases, computation time also increases for both the models but comparatively PrinciResNet16 model has less computation time.

The comparison table in Table V compares the proposed PrinciResNet16 method with other classification algorithms which are constructed on Principal Component Analysis, Discrete Wavelet Transform Learning search expansion, Data augmentation method, Hybrid GooLeNet, and deep learning method [22]. It is inferred that our proposed method performs more or equal to other existing algorithms with a minimum number of layers and ResNet blocks.

IV. Conclusion and Future Work

An automated classification system for distinguishing between Meningioma and Sarcoma brain tumors has been developed using a deep-learning model called PrinciResNet16. This model has been optimized for efficiency by employing a reduced number of layers and incorporating five skip connection blocks, which not only simplifies the ResNet architecture but also helps mitigate the vanishing gradient problem. Additionally, a preprocessing step involv-

ing the use of PCA is applied to the input multimodal image. This PCA technique reduces redundancy, creating a more energy-compact image for subsequent processing. The training dataset consists of 1600 slices, encompassing both single and fused image slices. This model achieves an impressive accuracy rate of 99% while requiring less computational time compared to a ResNet16 model without skip connections. Furthermore, other performance metrics such as sensitivity and specificity also yield promising results when compared against standard models. This robust model efficiently supports the classification of six distinct classes of multimodal Meningioma and Sarcoma brain tumors. However, there exists a trade-off between removing redundancy from the input image and preserving essential information and this balancing is crucial. Moreover, the model faces a challenge in sustaining its high accuracy when trained on larger datasets of brain tumor images. To further expand this work, future directions could include extending the classification capabilities to encompass other brain tumor types like Glioma and Pituitary tumors. Additionally, there is potential for incorporating effective segmentation techniques to identify and delineate tumor regions within the images.

References

[1] H. Kibriya, R. Amin, A. H. Alshehri, M. Masood, S. S. Alshamrani, and A. Alshehri, "A novel and effective brain tumor classification model using deep feature fusion and famous machine learning classifiers," *Comput. Intell. Neurosci.*, vol. 2022, pp. 1–15, 2022.

[2] J. Amin, M. Sharif, A. Haldorai, M. Yasmin, and R. S. Nayak, "Brain tumor detection and classification using machine learning: a comprehensive survey," *Complex Intell. Syst.*, vol. 8, no. 4, pp. 3161–3183, 2022.

[3] E. Irmak, "Multi-classification of brain tumor MRI images using deep convolutional neural network with fully optimized framework," *Iran. J. Sci. Technol. Trans. Electr. Eng.*, vol. 45, p. 3, 2021.

[4] M. Padma Usha, G. Kannan, and M. Ramamoorthy, *Multimodal Image Fusion with Segmentation for Detection of Brain Tumor Using Deep Learning Algorithm*. Apple Academic Press, 2023.

[5] M. Rasool, N. A. Ismail, W. Boulila, A. Ammar, H. Samma, W. M. S. Yafooz, and A. M. Emara, "A hybrid deep learning model for brain tumour classification," *Entropy (Basel)*, vol. 24, no. 6, p. 799, 2022.

[6] S. Saeedi, S. Rezayi, H. Keshavarz, and S. R. N. Kalhori, "MRI-based brain tumor detection using convolutional deep learning methods and chosen machine learning techniques," *BMC Med. Inform. Decis. Mak.*, vol. 23, no. 1, p. 16, 2023.

[7] M. Ramamoorthy, S. Qamar, R. Manikandan, N. Z. Jhanjhi, M. Masud, and M. A. AlZain, "Earlier detection of brain tumor by preprocessing based on histogram equalization with neural network," *Healthcare*, vol. 10, no. 7, p. 1218, 2022.

[8] M. Padma Usha, G. Kannan, and M. Ramamoorthy, "An efficient berkeley's wavelet convolutional transfer learning and local binary gabor fuzzy C-means clustering for brain tumour detection," *Imaging Sci. J.*, pp. 1–14, 2023.

[9] I. E. Kaya, A. Ç. Pehlivanli, E. G. Sekizkardeş, and T. Ibrikci, "PCA based clustering for brain tumor segmentation of T1w MRI images," *Comput. Methods Programs Biomed.*, vol. 140, pp. 19–28, 2017.

[10] B. Zhao, X. Dong, Y. Guo, X. Jia, and Y. Huang, "PCA dimensionality reduction method for image classification," *Neural Process. Lett.*, vol. 54, no. 1, pp. 347–368, 2022.

[11] M. K. Islam, M. S. Ali, M. S. Miah, M. M. Rahman, M. S. Alam, and M. A. Hossain, "Brain tumor detection in MR image using superpixels, principal component analysis and template based K-means clustering algorithm," *Mach. Learn. Appl.*, vol. 5, p. 100044, 2021.

[12] Z. Liu, L. Tong, L. Chen, Z. Jiang, Q. Z. F. Zhou, X. Zhang, Y. Jin, and H. Zhou, "Deep learning based brain tumor segmentation: a survey," *Complex Intell. Syst.*, vol. 9, pp. 1001–1026, 2023.

[13] S. B. Gaikwad and M. S. Joshi, "Brain tumor classification using principal component analysis and probabilistic neural network," *Int. J. Comput. Appl.*, vol. 120, no. 3, pp. 5–9, 2015.

[14] S. C. Ng, "Principal component analysis to reduce dimension on digital image," *Procedia Comput. Sci.*, vol. 111, pp. 113–119, 2017.

[15] M. Padma Usha, G. Kannan, M. Ramamoorthy, M. Sharmila, G. A. Huzaifa Anjum, and M. S. H. Hairunnisha, "Multimodal brain image fusion using graph intelligence method," *Int. J. Res. Pharm. Sci.*, vol. 11, no. 2, 2020.

[16] M. D. Keith, A. Johnson, and J. A. Becker, https://www.med.harvard.edu/aanlib/, Accessed: Dec. 12, 2021.

[17] Navoneel Chakraborty, https://www.kaggle.com/datasets/navoneel/brain-mri-images-for-brain-tumor-detection, Accessed: Dec. 21, 2021.

[18] S. Arora, M. Hanmandlu, and G. Gupta, "Filtering impulse noise in medical images using information sets," *Pattern Recognit. Lett.*, vol. 139, pp. 1–9, 2020.

[19] D. Nandi, A. S. Ashour, S. Samanta, S. Chakraborty, M. A. M. Salem, and N. Dey, "Principal component analysis in medical image processing: a study," *Int. J. Image Min.*, vol. 1, no. 1, p. 65, 2015.

[20] P. Suetens, *Fundamentals of medical imaging*, 2nd ed. Cambridge University Press, 2009.

[21] E. S. A. El-Dahshan, T. Hosny, and A. B. M. Salem, "Hybrid intelligent techniques for MRI brain images classification," *Digit. Signal Process.*, vol. 20, no. 2, pp. 433–441, 2010.

[22] M. Ahmed Hamza, H. Abdullah Mengash, S. S. Alotaibi, S. B. H. Hassine, A. Yafoz, F. Althukair, M. Othman, and R. Marzouk, "Optimal and efficient deep learning model for brain tumor magnetic resonance imaging classification and analysis," *Appl. Sci.*, vol. 12, no. 15, p. 7953, 2022.

[23] H. Zhang, J. Mo, H. Jiang, Z. Li, W. Hu, C. Zhang, Y. Wang, X. Wang, C. Liu, B. Zhao, J. Zhang, and K. Zhang, "Deep learning model for the automated detection and histopathological prediction of meningioma," *Neuroinformatics*, vol. 19, no. 3, pp. 393–402, 2021.

[24] M. Gao, D. Qi, H. Mu, and J. Chen, "A transfer residual neural network based on ResNet-34 for detection of wood knot defects," *Forests*, vol. 12, no. 2, p. 212, 2021.

[25] L. Zhao, J. Ma, Y. Shao, C. Jia, J. Zhao, and H. Yuan, "MM-UNet: A multimodality brain tumor segmentation network in MRI images," *Front. Oncol.*, vol. 12, p. 950706, 2022.

[26] S. Chitnis, R. Hosseini, and P. Xie, "Brain tumor classification based on neural architecture search," *Sci. Rep.*, vol. 12, no. 1, p. 19206, 2022.

[27] J. Cheng, W. Huang, S. Cao, R. Yang, W. Yang, Z. Yun, Z. Wang, and Q. Feng, "Enhanced performance of brain tumor classification via tumor region augmentation and partition," *PLoS ONE*, vol. 10, no. 10, p. e0140381, 2015.

[28] S. Kokkalla, J. Kakarla, I. B. Venkateswarlu, and M. Singh, "Three-class brain tumor classification using deep dense inception residual network," *Soft Comput.*, vol. 25, no. 13, pp. 8721–8729, 2021.

Ms. M. Padma Usha received a Master of Engineering in Communication Systems from Anna University, Chennai, India in the year 2008. She completed her undergraduate in B.Tech Electronics at Madras Institute of Technology, Chennai in the year 2005. Currently, she is working as an Assistant Professor (Senior Grade) in the Department of Electronics and Communication Engineering of B.S.Abdur Rahman Crescent Institute of Science and Technology Chennai, India. She has fourteen years of teaching experience. She currently works in the domain of Medical image processing and Artificial Intelligence.

Dr. G. Kannan received a Ph.D. degree from Anna University Chennai, India, an M.Tech in Embedded Systems from SASTRA University Thanjavur, and B.E Electronics and Instrumentation Engineering from Bharadhidasan University Tiruchirappalli in the year 2014, 2005, and 2000 respectively. At present, he is working as an Associate Professor in the Department of Electronics and Communication Engineering of B.S.Abdur Rahman Crescent Institute of Science and Technology Chennai, India. He has 15 years of teaching & research experience and his areas of research include Wireless Sensor Networks, System level power management in Embedded Systems, Real-Time Operating Systems, and Artificial Intelligence.

Mr. S. Sai Akshay is currently pursuing his B.Tech degree in the Electronics and Communications department at B.S. Abdur Rahman Institute of Science and Technology, Vandalur, Chennai. His areas of interest are Data Science, Machine Learning, and Image Processing.

Mr. S. Giri is currently pursuing his B.Tech degree in the Electronics and Communications department at B.S. Abdur Rahman Institute of Science and Technology, Vandalur, Chennai. His areas of interest are Image Processing, Automation, and Embedded Systems.

Mr. Shaik Muhammad Huzaifa is currently pursuing his B.Tech degree in the Electronics and Communications department at B.S. Abdur Rahman Institute of Science and Technology, Vandalur, Chennai. His areas of interest are Python Development and Data Science.